Available online at www.sciencedirect.com
ScienceDirect
Journal of Solid State Chemistry 179 (2006) 3776–3783
JOURNAL OF SOLID STATE CHEMISTRY
www.elsevier.com/locate/jssc

Structure and physical properties of rare-earth zinc antimonides $RE\mathrm{Zn}_{1-x}\mathrm{Sb}_2$ (RE = La, Ce, Pr, Nd, Sm, Gd, Tb)

Oksana Ya. Zelinska[a,b], Arthur Mar[a,*]

[a]Department of Chemistry, University of Alberta, Edmonton, Alberta, Canada T6G 2G2
[b]Department of Inorganic Chemistry, Ivan Franko National University of Lviv, 79005 Lviv, Ukraine

Received 23 June 2006; received in revised form 10 August 2006; accepted 12 August 2006
Available online 17 August 2006

Abstract

The ternary rare-earth zinc antimonides $RE\mathrm{Zn}_{1-x}\mathrm{Sb}_2$ (RE = La, Ce, Pr, Nd, Sm, Gd, Tb) were prepared by heating at 1050 °C followed by annealing at 600 °C. For all members, single-crystal X-ray diffraction studies indicated that the Zn deficiency is essentially fixed, corresponding to the formula $RE\mathrm{Zn}_{0.6}\mathrm{Sb}_2$, with no appreciable homogeneity range. These compounds adopt the HfCuSi_2-type structure (Pearson symbol $tP8$, space group $P4/nmm$, $Z = 2$). Single-crystal electrical resistivity measurements confirmed the occurrence of an abrupt resistivity decrease near 4 K for RE = Ce, and a less pronounced one for RE = La, Pr, and Gd. Except for the ferromagnetic Ce ($T_c = 2.5$ K) and antiferromagnetic Tb ($T_N = 10$ K) members, all remaining compounds exhibit no long-range magnetic ordering down to 2 K, instead showing temperature-independent (RE = La), van Vleck (RE = Sm), or Curie–Weiss paramagnetism (RE = Pr, Nd, Gd).

Keywords: Antimonide; Crystal structure; Magnetic properties; Transport properties

1. Introduction

Ternary antimonides containing rare-earth (RE) and transition metals (M) represent an emerging class of materials possessing a wide variety of physical properties. The most prominent examples are the RE filled skutterudites derived from $RE\mathrm{Fe}_4\mathrm{Sb}_{12}$, which form the basis for new thermoelectric materials [1]. However, other phases also possess potentially interesting electrical and magnetic properties. A comprehensive review of the structures and properties of these ternary antimonides is available [2].

In particular, an extensive series of ternary antimonides with the composition $REM_{1-x}\mathrm{Sb}_2$ is known for many RE and transition metals [2]. In nearly all cases, where structures have been refined, there is a significant deficiency of the M site in the parent tetragonal HfCuSi_2-type structure (Pearson symbol $tP8$). In some of the corresponding arsenides $REM_{1-x}\mathrm{As}_2$, superstructures of the HfCuSi_2-type have been identified in which the symmetry is reduced from tetragonal to orthorhombic as a result of metal vacancy ordering [3] or of distortions of the square pnicogen net [4]. Given the layered nature of the crystal structure and the substitutional breadth possible in the transition-metal site (M = Mn, Fe, Co, Ni, Pd, Cu, Ag, Au, Zn, Cd) [2], the $REM_{1-x}\mathrm{Sb}_2$ compounds are attractive candidates for disclosing a variety of magnetic and transport properties. In general, ferromagnetic ordering has been reported for M = Mn ($T_C = 130$–520 K) [5] although this has been disputed [6], antiferromagnetic ordering for M = Ni, Pd, Cu, Ag, Au ($T_N = 3$–20 K) [7–10], and no long-range magnetic ordering for M = Cd down to 2 K [11]. For the remaining members, magnetic measurements have so far been limited to the Ce representatives [12].

The Zn-containing compounds were among the earliest members to be discovered, forming for RE = La, Ce, Pr, Nd, Sm, Gd, Tb [5,12–15], but they remain incompletely characterized. The definitive composition for $\mathrm{LaZn}_{0.52(2)}\mathrm{Sb}_2$ has apparently been established by single-crystal X-ray diffraction [13]. The Ce member has been variously reported as $\mathrm{CeZn}_{0.6}\mathrm{Sb}_2$ [12] or $\mathrm{CeZn}_{0.81(3)}\mathrm{Sb}_2$ [15], from powder

*Corresponding author. Fax: +1 780 492 8231.
E-mail address: arthur.mar@ualberta.ca (A. Mar).

0022-4596/$ - see front matter © 2006 Elsevier Inc. All rights reserved.
doi:10.1016/j.jssc.2006.08.011

X-ray diffraction studies. Evidence for a distortion to the orthorhombic $NdAgSb_2$-type structure has been observed for $LaZn_{0.6}Sb_2$ and $CeZn_{0.8}Sb_2$ when they are annealed at higher temperatures [15]. Physical properties have been measured only for the Ce member so far [5,12,16]. $CeZn_{0.6}Sb_2$ was first suggested to be antiferromagnetic ($T_N = 2.0$ K) [12], but recent reports indicate the presence of both ferromagnetic (within the *ab* plane) and antiferromagnetic (along *c*) transitions, as well as a pressure-induced resistivity anomaly [16,17].

We report here single-crystal X-ray diffraction studies on the entire $RECn_{1-x}Sb_2$ series to ascertain the precise composition of each member, and we characterize their properties through electrical resistivity and magnetic susceptibility measurements.

2. Experimental

2.1. Synthesis

Starting materials were powders of the *RE* metals (99.9%, Cerac or Aldrich), Zn (99.9%, Cerac), and Sb (99.999%, Alfa-Aesar). Products were characterized by powder X-ray diffraction patterns collected on an Inel powder diffractometer equipped with a CPS 120 detector. Elemental compositions were determined by energy-dispersive X-ray (EDX) analysis with use of a Hitachi S-2700 scanning electron microscope.

In optimized syntheses, $RECn_{1-x}Sb_2$ samples were prepared by reacting *RE*, Zn, and Sb in a 1:0.7:2 mol ratio for *RE* = La, Ce, Pr, Nd, and Sm, and in a 1:1:2 mol ratio for *RE* = Gd and Tb. The reactants were placed in evacuated fused-silica tubes, which were heated at 650 °C for 12 h and at 1050 °C for 6 h, cooled slowly to 600 °C at a rate of 4 °C/h, further annealed at 600 °C over 8*d*, and then quenched in cold water. For *RE* = Gd and Tb, the use of a slight Zn excess minimizes the formation of binary *RE*–Sb and Zn–Sb phases, presumably by avoiding a peritectic decomposition that would otherwise occur at the stoichiometric composition. These reactions yielded plate-shaped single crystals, which were confirmed by EDX measurements to contain the elements in the expected proportions and with an appreciable deficiency of Zn (Table 1).

Additional reactions with nominal compositions $LaZn_{0.4}Sb_2$, $LaZn_{0.5}Sb_2$, and $LaZn_{0.6}Sb_2$ were conducted under the same heating conditions as above to determine the phase width in $LaZn_{1-x}Sb_2$. Table 2 lists the cell parameters of the ternary phase refined from the powder patterns. The negligible variation of the cell parameters implies that there is no significant homogeneity range in $LaZn_{1-x}Sb_2$, confirming an earlier assertion [13]. Moreover, the powder patterns from reactions with loading compositions $LaZn_{0.4}Sb_2$ and $LaZn_{0.5}Sb_2$ indicated the presence of trace amounts of binary phases, in addition to the major ternary phase.

Table 1
EDX analysis of $RECn_{1-x}Sb_2$ crystals

Loading composition	Elemental analysis (at%)		
	RE	Zn	Sb
$LaZn_{0.7}Sb_2$	27(2)	20(2)	53(2)
$CeZn_{0.7}Sb_2$	26(2)	23(2)	51(2)
$PrZn_{0.7}Sb_2$	28(2)	21(2)	51(2)
$NdZn_{0.7}Sb_2$	28(2)	19(2)	53(2)
$SmZn_{0.7}Sb_2$	29(2)	19(2)	52(2)
$GdZnSb_2$	30(3)	19(3)	51(3)
$TbZnSb_2$	29(2)	19(2)	52(2)

Table 2
Cell parameters for the ternary phase from reactions with loading composition $LaZn_{1-x}Sb_2$[a]

Loading composition	*a* (Å)	*c* (Å)	*V* (Å^3)
$LaZn_{0.4}Sb_2$	4.394	10.517	203.1
$LaZn_{0.5}Sb_2$	4.392	10.515	202.9
$LaZn_{0.6}Sb_2$	4.394	10.518	203.1
$LaZn_{0.7}Sb_2$	4.382	10.494	201.5

[a]Standard uncertainties are <0.001 Å for *a* and *c* and <0.1 Å^3 for *V*.

2.2. Structure determination

Single-crystal X-ray intensity data for $RECn_{1-x}Sb_2$ (*RE* = La, Ce, Pr, Nd, Sm, Gd, Tb) were collected on a Bruker Platform/SMART 1000 CCD diffractometer at 22 °C using ω scans. Crystal data and further details of the data collection are given in Table 3. Calculations were carried out with use of the SHELXTL (version 6.12) package [18]. Face-indexed numerical absorption corrections were applied. The centrosymmetric space group *P*4/*nmm* was chosen and initial atomic positions were found by direct methods, confirming the expected $HfCuSi_2$-type structure. The powder X-ray diffraction patterns did not reveal any splitting of diffraction peaks and the single-crystal diffraction data did not show additional superstructure reflections that might be suggestive of lower symmetry. The atomic positions were standardized with the program STRUCTURE TIDY [19]. Refinements proceeded in a straightforward manner, with partial occupancy being found only in the Zn site (2*b*). Final values of the positional and displacement parameters are given in Table 4. Selected interatomic distances and angles are listed in Table 5. Further data, in the form of a CIF, have been sent to Fachinformationszentrum Karlsruhe, Abt. PROKA, 76344 Eggenstein-Leopoldshafen, Germany, as supplementary material No. CSD-416870 to 416876 and can be obtained by contacting FIZ (quoting the article details and the corresponding CSD numbers).

2.3. Property measurements

The electrical resistivity within the *ab* plane (ρ_{ab}) of silver plate-shaped crystals was measured from 2 to 300 K by

Table 3
Crystallographic data for $REZn_{1-x}Sb_2$ (RE = La, Ce, Pr, Nd, Sm, Gd, Tb)

Formula	$LaZn_{0.609(4)}Sb_2$	$CeZn_{0.651(4)}Sb_2$	$PrZn_{0.635(7)}Sb_2$	$NdZn_{0.614(6)}Sb_2$	$SmZn_{0.615(7)}Sb_2$	$GdZn_{0.611(5)}Sb_2$	$TbZn_{0.612(6)}Sb_2$
Formula mass (amu)	422.29	426.11	425.59	427.62	434.38	440.63	442.30
Space group	$P4/nmm$ (No. 129)	$P4/nmm$ (No. 129)	$P4/nmm$ (No. 129)	$P4/nmm$ (No. 129)	$P4/nmm$ (No. 129)	$P4/nmm$ (No. 129)	$P4/nmm$ (No. 129)
a (Å)	4.3857(4)	4.3626(6)	4.3397(5)	4.3250(4)	4.2963(4)	4.2740(5)	4.2581(5)
c (Å)	10.5000(9)	10.4150(13)	10.3578(13)	10.3291(10)	10.2664(10)	10.2630(11)	10.2309(12)
V (Å^3)	201.96(3)	198.22(5)	195.07(4)	193.21(3)	189.50(3)	187.48(4)	185.50(4)
Z	2	2	2	2	2	2	2
ρ_{calcd} (g cm^{-3})	6.944	7.139	7.246	7.350	7.613	7.806	7.919
Crystal dimensions (mm)	0.19 × 0.12 × 0.02	0.13 × 0.13 × 0.01	0.20 × 0.11 × 0.08	0.16 × 0.12 × 0.08	0.24 × 0.10 × 0.03	0.10 × 0.09 × 0.04	0.08 × 0.08 × 0.02
Radiation	Graphite monochromated Mo$K\alpha$, $\lambda = 0.71073$ Å	Graphite monochromated Mo$K\alpha$, $\lambda = 0.71073$ Å	Graphite monochromated Mo$K\alpha$, $\lambda = 0.71073$ Å	Graphite monochromated Mo$K\alpha$, $\lambda = 0.71073$ Å	Graphite monochromated Mo$K\alpha$, $\lambda = 0.71073$ Å	Graphite monochromated Mo $K\alpha$, $\lambda = 0.71073$ Å	Graphite monochromated Mo$K\alpha$, $\lambda = 0.71073$ Å
μ(Mo$K\alpha$) (cm^{-1})	269.50	284.02	295.61	305.51	330.06	353.27	368.89
Transmission factors	0.066–0.512	0.066–0.710	0.048–0.158	0.016–0.150	0.041–0.423	0.069–0.258	0.113–0.474
2θ limits	$3.88° \leqslant 2\theta(\text{Mo}K\alpha) \leqslant 66.30°$	$3.92° \leqslant 2\theta(\text{Mo}K\alpha) \leqslant 66.40°$	$3.94° \leqslant 2\theta(\text{Mo } K\alpha) \leqslant 66.30°$	$3.94° \leqslant 2\theta(\text{Mo } K\alpha) \leqslant 65.88°$	$3.96° \leqslant 2\theta(\text{Mo } K\alpha) \leqslant 66.14°$	$3.96° \leqslant 2\theta(\text{Mo } K\alpha) \leqslant 66.30°$	$3.98° \leqslant 2\theta(\text{Mo } K\alpha) \leqslant 66.16°$
Data collected	$-6 \leqslant h \leqslant 6$, $-6 \leqslant k \leqslant 6$, $-16 \leqslant l \leqslant 15$	$-6 \leqslant h \leqslant 6$, $-6 \leqslant k \leqslant 6$, $-15 \leqslant l \leqslant 15$	$-6 \leqslant h \leqslant 6$, $-6 \leqslant k \leqslant 6$, $-15 \leqslant l \leqslant 15$	$-6 \leqslant h \leqslant 6$, $-6 \leqslant k \leqslant 6$, $-15 \leqslant l \leqslant 15$	$-6 \leqslant h \leqslant 6$, $-6 \leqslant k \leqslant 6$, $-15 \leqslant l \leqslant 15$	$-6 \leqslant h \leqslant 6$, $-6 \leqslant k \leqslant 6$, $-15 \leqslant l \leqslant 15$	$-6 \leqslant h \leqslant 6$, $-6 \leqslant k \leqslant 6$, $-15 \leqslant l \leqslant 15$
No. of data collected	2735	2690	2545	2181	2575	2574	2499
No. of unique data, including $F_o^2 < 0$	271	266	265	260	260	258	253
No. of unique data, with $F_o^2 > 2\sigma(F_o^2)$	265	255	262	258	260	242	245
No. of variables	13	13	13	13	13	13	13
$R(F)$ for $F_o^2 > 2\sigma(F_o^2)$[a]	0.017	0.016	0.027	0.019	0.020	0.017	0.017
$R_w(F_o^2)$[b]	0.041	0.034	0.070	0.044	0.049	0.037	0.039
Goodness of fit	1.224	1.259	1.442	1.311	1.174	1.143	1.253
$(\Delta\rho)_{max}$, $(\Delta\rho)_{min}$ (e Å^{-3})	1.27, −1.98	1.05, −1.09	2.12, −2.24	1.46, −2.18	2.01, −1.95	1.25, −1.64	2.29, −1.45

[a] $R(F) = \Sigma||F_o| - |F_c||/\Sigma|F_o|$.
[b] $R_w(F_o^2) = [\Sigma[w(F_o^2 - F_c^2)^2]/\Sigma wF_o^4]^{1/2}$; $w^{-1} = [\sigma^2(F_o^2) + (Ap)^2 + Bp]$ where $p = [\max(F_o^2, 0) + 2F_c^2]/3$.

Table 4
Atomic coordinates and equivalent isotropic displacement parameters ($Å^2$) [a] for $RE\mathrm{Zn}_{1-x}\mathrm{Sb}_2$ (RE = La, Ce, Pr, Nd, Sm, Gd, Tb)

	$LaZn_{0.609(4)}Sb_2$	$CeZn_{0.651(4)}Sb_2$	$PrZn_{0.635(7)}Sb_2$	$NdZn_{0.614(6)}Sb_2$	$SmZn_{0.615(7)}Sb_2$	$GdZn_{0.611(5)}Sb_2$	$TbZn_{0.612(6)}Sb_2$
RE in 2c ($\frac{1}{4}$, $\frac{1}{4}$, z)							
z	0.24271(3)	0.23953(4)	0.24065(6)	0.23981(4)	0.23945(5)	0.23793(4)	0.23692(4)
U_{eq}	0.01086(13)	0.01055(11)	0.0101(2)	0.01089(16)	0.00988(17)	0.01068(12)	0.01042(13)
Zn in 2b ($\frac{3}{4}$, $\frac{1}{4}$, $\frac{1}{2}$)							
occupancy	0.609(4)	0.651(4)	0.635(7)	0.614(6)	0.615(7)	0.611(5)	0.612(6)
U_{eq}	0.0167(4)	0.0172(4)	0.0168(7)	0.0159(5)	0.0154(6)	0.0164(5)	0.0165(5)
Sb1 in 2c ($\frac{1}{4}$, $\frac{1}{4}$, z)							
z	0.65308(4)	0.65707(5)	0.65789(7)	0.65916(5)	0.66109(6)	0.66249(5)	0.66384(5)
U_{eq}	0.01171(14)	0.01135(12)	0.0108(3)	0.01135(17)	0.01001(19)	0.01031(14)	0.00974(15)
Sb2 in 2a ($\frac{3}{4}$, $\frac{1}{4}$, 0)							
U_{eq}	0.01103(13)	0.01038(12)	0.0097(2)	0.01035(16)	0.00896(18)	0.00930(13)	0.00874(14)

[a] U_{eq} is defined as one-third of the trace of the orthogonalized U_{ij} tensor.

Table 5
Selected interatomic distances (Å) and angles (deg) for $RE\mathrm{Zn}_{1-x}\mathrm{Sb}_2$ (RE = La, Ce, Pr, Nd, Sm, Gd, Tb)

	$LaZn_{0.609(4)}Sb_2$	$CeZn_{0.651(4)}Sb_2$	$PrZn_{0.635(7)}Sb_2$	$NdZn_{0.614(6)}Sb_2$	$SmZn_{0.615(7)}Sb_2$	$GdZn_{0.611(5)}Sb_2$	$TbZn_{0.612(6)}Sb_2$
RE–Sb1 ($\times 4$)	3.2885(3)	3.2674(4)	3.2436(5)	3.2314(4)	3.2049(4)	3.1903(4)	3.1775(4)
RE–Sb2 ($\times 4$)	3.3620(3)	3.3139(4)	3.3048(6)	3.2882(4)	3.2647(4)	3.2449(4)	3.2261(4)
RE–Zn ($\times 4$)	3.4795(3)	3.4810(4)	3.4532(6)	3.4495(4)	3.4307(5)	3.4353(4)	3.4318(5)
Zn–Sb1 ($\times 4$)	2.7188(3)	2.7266(4)	2.7171(5)	2.7164(4)	2.7110(4)	2.7107(4)	2.7097(4)
Zn–Zn ($\times 4$)	3.1012(3)	3.0848(4)	3.0686(4)	3.0582(3)	3.0379(3)	3.0222(4)	3.0109(4)
Sb2–Sb2 ($\times 4$)	3.1012(3)	3.0848(4)	3.0686(4)	3.0582(3)	3.0379(3)	3.0222(4)	3.0109(4)
Sb1–Zn–Sb1 ($\times 4$)	110.46(1)	111.10(1)	111.24(1)	111.48(1)	111.85(1)	112.24(1)	112.50(1)
Sb1–Zn–Sb1 ($\times 2$)	107.52(2)	106.26(2)	105.99(3)	105.52(2)	104.82(2)	104.06(2)	103.57(2)

standard four-probe techniques on a Quantum Design PPMS system equipped with an ac transport controller (Model 7100). The current was 100 μA and the frequency was 16 Hz. Magnetic susceptibility measurements were made on ground samples (~100 mg) on a Quantum Design 9T-PPMS dc magnetometer/ac susceptometer. The susceptibility was corrected for contributions for the holder diamagnetism and the underlying sample diamagnetism.

3. Results and discussion

Structure refinement for the $RE\mathrm{Zn}_{1-x}\mathrm{Sb}_2$ series reveals significant deficiency of the Zn site for all members, corresponding to the formula $RE\mathrm{Zn}_{\sim 0.6}\mathrm{Sb}_2$. The cell parameters for $LaZn_{0.609(4)}Sb_2$ ($a = 4.3857(4)$ Å, $c = 10.5000(9)$ Å) obtained here are close to those previously reported for $LaZn_{0.52(2)}Sb_2$ ($a = 4.380(3)$ Å, $c = 10.488(5)$ Å) [13] and $LaZn_{0.62(3)}Sb_2$ ($a = 4.3893(2)$ Å, $c = 10.5072(5)$ Å) [15], which were prepared in an excess of Zn. Further syntheses in the $LaZn_{1-x}Sb_2$ system revealed no significant variation in the cell parameters (Table 2), supporting a composition fixed at $LaZn_{0.6}Sb_2$. The same conclusion can be assumed for the other RE members, whose cell parameters are in good agreement with those reported earlier.

The defect $HfCuSi_2$-type structure adopted by $RE\mathrm{Zn}_{1-x}\mathrm{Sb}_2$ is built up by stacking layers of condensed $ZnSb_4$ tetrahedra alternating with square Sb nets, separated by RE atoms in square antiprismatic coordination (Fig. 1). As the cell parameters decrease smoothly as a function of RE (Fig. 2a), reflecting the lanthanide contraction, the bond lengths also decrease in a regular manner (Fig. 2b). In particular, the Zn–Zn or Sb2–Sb2 distances fall off in the same way as the RE–Zn or RE–Sb distances, indicating that the contraction of the square arrays of Zn or Sb2 atoms appears to result simply from a size effect. However, the contraction does not proceed indefinitely. In fact, the Sb2–Sb2 distances within the square net never fall below ~3.0 Å in all $REM_{1-x}Sb_2$ structures examined. Another part of the structure must also be able to respond upon RE substitution, and this occurs through distortion of the M-centred tetrahedra. Inspection of the Sb–Zn–Sb angles in $RE\mathrm{Zn}_{1-x}\mathrm{Sb}_2$ shows that the $ZnSb_4$ tetrahedra are slightly elongated along c and become more so on progressing from the La (110.46(1)° ($\times 4$), 107.52(2)° ($\times 2$)) to the Tb member (112.50(1)° ($\times 4$), 103.57(2)° ($\times 2$)), while the Zn–Sb distances remain relatively constant at ~2.71 Å (Table 5). The degree of distortion appears to be related to the breadth of RE substitution possible in a given $REM_{1-x}Sb_2$ series. In general, the tetrahedral distortion is more pronounced when M is larger. For example, whereas $RE\mathrm{Zn}_{1-x}\mathrm{Sb}_2$ series forms for RE = La–Nd, Sm, Gd, Tb, the $RE\mathrm{Cd}_{1-x}\mathrm{Sb}_2$ series forms for RE = La–Nd, Sm [11]. The limiting member of the $RE\mathrm{Cd}_{1-x}\mathrm{Sb}_2$ series,

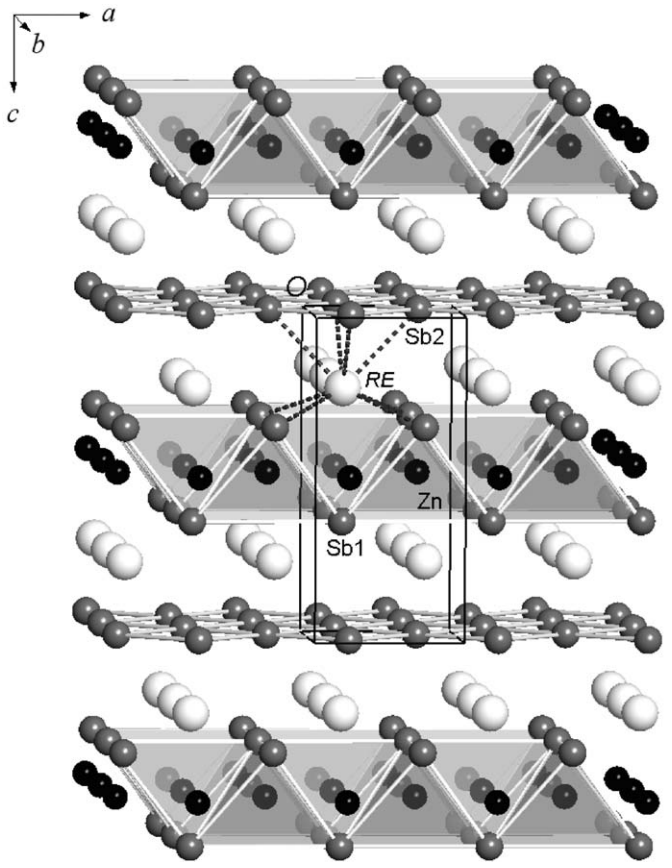

Fig. 1. Structure of $RE\mathrm{Zn}_{1-x}\mathrm{Sb}_2$, viewed approximately down the *b*-axis.

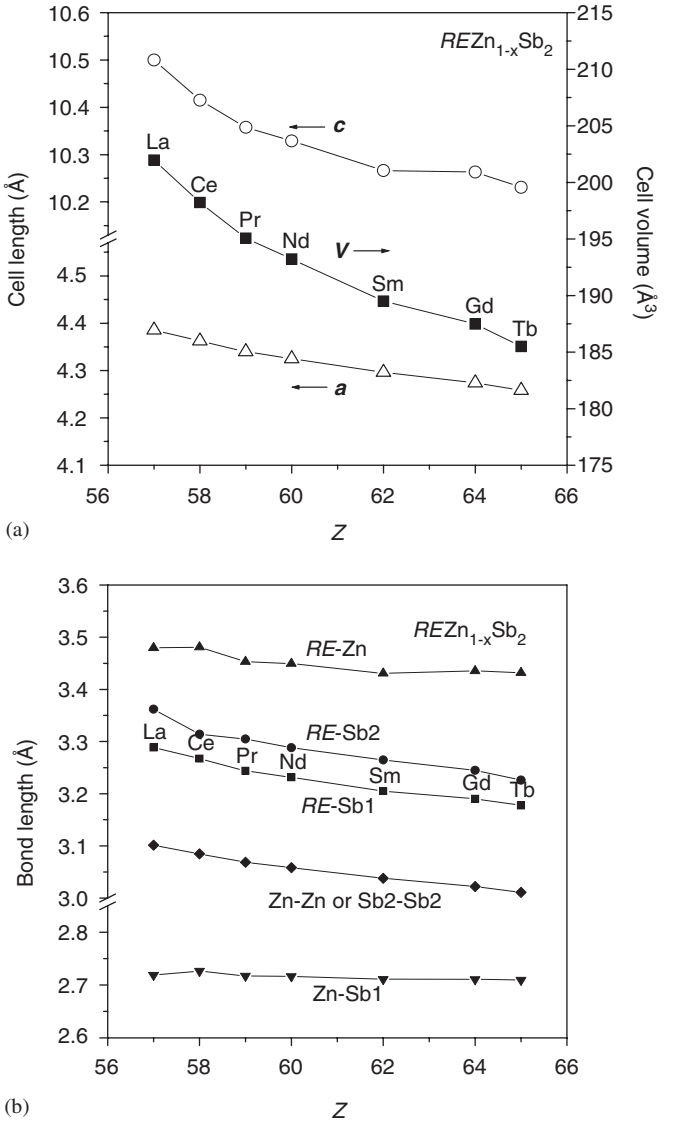

Fig. 2. Plots of (a) cell parameters and (b) bond lengths as a function of *RE* in the $RE\mathrm{Zn}_{1-x}\mathrm{Sb}_2$ series.

$\mathrm{SmCd}_{0.6}\mathrm{Sb}_2$, contains Sb–Cd–Sb angles (116.49(1)° ($\times 4$), 96.19(2)° ($\times 2$)) [11] that deviate significantly from the ideal tetrahedral values, compared to those for any member of the $RE\mathrm{Zn}_{1-x}\mathrm{Sb}_2$ series.

The bonding in $REM_{1-x}\mathrm{Sb}_2$ compounds cannot be explained in a simple way by Zintl's rules. Conventionally, the idealized formulation $(RE^{3+})(M^{2+})_{0.5}(\mathrm{Sb1})^{3-}(\mathrm{Sb2})^{1-}$ has been invoked to account for the presence of defects in the transition-metal site when *M* is a dipositive cation [20] as is the case here for $RE\mathrm{Zn}_{1-x}\mathrm{Sb}_2$, but exact half-occupancy is not observed experimentally. A band structure calculation has been performed on CaZnSb_2 [21], which is isostructural and isoelectronic (if only valence electrons are counted) to "$RE\mathrm{Zn}_{0.5}\mathrm{Sb}_2$". The Fermi level crosses partially filled bands derived by mixing of states in the [ZnSb] slab and the Sb square net. At this electron count, a pnicogen square net is prone to distortion, as has now been identified in some arsenides [4], but the greater overlap of metal and Sb states tends to suppress this distortion in the case of antimonides. The non-integral electron count observed in $RE\mathrm{Zn}_{1-x}\mathrm{Sb}_2$ and related compounds, which can be accommodated by further slight reduction of the Sb2 atoms within the pnicogen square net, may correspond to an optimal value that stabilizes the undistorted structure. Vacancy ordering of the transition metal site has been observed in the ternary arsenide $\mathrm{Pr}_3\mathrm{Zn}_2\mathrm{As}_6$ (or $\mathrm{PrZn}_{0.67}\mathrm{As}_2$) and has been proposed to arise from avoidance of antibonding Zn–Zn interactions [3]. In the case of the antimonides here, the Zn–Zn distances are always greater than 3.0 Å and pose no destabilizing interactions, so there is no strong driving force for such ordering.

Table 6 summarizes the electrical and magnetic properties of $RE\mathrm{Zn}_{0.6}\mathrm{Sb}_2$. Plots of the in-plane electrical resistivity (ρ_{ab}) of single crystals are shown in Fig. 3. With the exception of the Gd member, there is a general trend towards lower resistivity values on progressing from $\mathrm{LaZn}_{0.6}\mathrm{Sb}_2$ to $\mathrm{TbZn}_{0.6}\mathrm{Sb}_2$, as was also observed in the $RE\mathrm{Cd}_{1-x}\mathrm{Sb}_2$ series [11]. This may reflect better orbital overlap and wider bands as the structure contracts. The resistivity of $\mathrm{CeZn}_{0.6}\mathrm{Sb}_2$ decreases abruptly near 4 K, close to the anomaly recently identified as arising from Kondo lattice behavior [16]. Interestingly, $\mathrm{LaZn}_{0.6}\mathrm{Sb}_2$,

Table 6
Physical properties of $RE\mathrm{Zn}_{1-x}\mathrm{Sb}_2$ (RE = La, Ce, Pr, Nd, Sm, Gd, Tb)

Compound	$\rho_{ab,\ 300}$ (μΩ cm)	χ_o (emu/mol)	θ_p (K)	$\mu_{\mathrm{eff,\ meas}}$ (μ_B)	$\mu_{\mathrm{eff,\ theor}}$ (μ_B)
$\mathrm{LaZn}_{0.6}\mathrm{Sb}_2$	35	4.6×10^{-4} (TIP)			
$\mathrm{CeZn}_{0.6}\mathrm{Sb}_2$	28	2.1×10^{-3}	+1.2	2.24	2.54
$\mathrm{PrZn}_{0.6}\mathrm{Sb}_2$	20	9.1×10^{-4}	+0.6	3.18	3.58
$\mathrm{NdZn}_{0.6}\mathrm{Sb}_2$	9	1.5×10^{-3}	−8.8	3.10	3.62
$\mathrm{SmZn}_{0.6}\mathrm{Sb}_2$	8	1.2×10^{-3}			
$\mathrm{GdZn}_{0.6}\mathrm{Sb}_2$	46	0	−29.8	6.90	7.94
$\mathrm{TbZn}_{0.6}\mathrm{Sb}_2$	7	0	−17.4	9.83	9.72

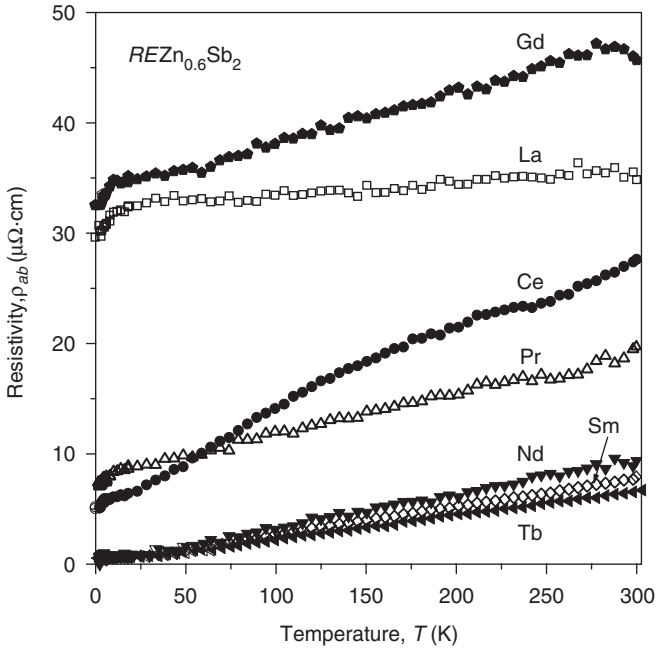

Fig. 3. Electrical resistivity of single crystals of $RE\mathrm{Zn}_{0.6}\mathrm{Sb}_2$ measured within the *ab* plane.

$\mathrm{GdZn}_{0.6}\mathrm{Sb}_2$, and to a lesser extent $\mathrm{PrZn}_{0.6}\mathrm{Sb}_2$ also exhibit a resistivity decrease at similar temperatures, although there is no obvious magnetic transition coincident with this feature.

Plots of the magnetic data are shown in Fig. 4. Except for $\mathrm{CeZn}_{0.6}\mathrm{Sb}_2$ and possibly $\mathrm{TbZn}_{0.6}\mathrm{Sb}_2$, none of these compounds shows long-range magnetic ordering down to 2 K. $\mathrm{LaZn}_{0.6}\mathrm{Sb}_2$ shows essentially temperature-independent Pauli paramagnetism (Fig. 4a), with a susceptibility value (4.6×10^{-4} emu/mol) that is nearly identical to that in $\mathrm{LaCd}_{0.6}\mathrm{Sb}_2$ (4.7×10^{-4} emu/mol) [11]. $\mathrm{CeZn}_{0.6}\mathrm{Sb}_2$ undergoes long-range ferromagnetic ordering, as signalled by the rapid increase in susceptibility at low temperatures (Fig. 4b) and the saturation behavior in the isothermal magnetization curve at 2 K (Fig. 4c). The ferromagnetic ordering temperature is pinpointed to be 2.5 K from ac magnetic susceptibility measurements (not shown), in good agreement with the transition temperatures (2.5 or 3.6 K) identified by Fisk et al. [16,17], and close to that found in ferromagnetic $\mathrm{CeCd}_{0.7}\mathrm{Sb}_2$ (2.8 K) [11]. Because the inverse magnetic susceptibility shows a pronounced curvature (inset of Fig. 4b), it was fit to the modified Curie–Weiss law ($\chi = C/(T-\theta_p)+\chi_o$), leading to an effective moment that is slightly smaller than the free-ion value for Ce^{3+}, a slightly positive Weiss constant consistent with ferromagnetic coupling, and a relative large temperature-independent contribution consistent with metallic conductivity (Table 6). $\mathrm{PrZn}_{0.6}\mathrm{Sb}_2$ and $\mathrm{NdZn}_{0.6}\mathrm{Sb}_2$ are paramagnetic, with the inverse magnetic susceptibility plots showing less pronounced curvature (Figs. 4d and e) and leading to effective magnetic moments obtained from fits to the modified Curie–Weiss law that are slightly depressed from the free-ion values for RE^{3+}. $\mathrm{SmZn}_{0.6}\mathrm{Sb}_2$ displays van Vleck paramagnetism typical of Sm-containing compounds and its susceptibility cannot be fit to the Curie–Weiss law (Fig. 4f). For $\mathrm{GdZn}_{0.6}\mathrm{Sb}_2$ and $\mathrm{TbZn}_{0.6}\mathrm{Sb}_2$, the inverse susceptibility curves are essentially linear (Figs. 4g and h) and were fit to the simple Curie–Weiss law. The $\mathrm{TbZn}_{0.6}\mathrm{Sb}_2$ sample contained ~10% impurities of TbSb, which is antiferromagnetic at $T_N = 16$ K [22]. Although attempts to prepare purer samples were unsuccessful, an additional shoulder was always observed at a somewhat lower temperature, near 10 K, which we attribute as intrinsic to $\mathrm{TbZn}_{0.6}\mathrm{Sb}_2$ itself. Measurements of the ac magnetic susceptibility confirmed the presence of this transition. For comparison, other $\mathrm{Tb}M_{1-x}\mathrm{Sb}_2$ compounds with the HfCuSi_2-type structure are also antiferromagnetic below similar transition temperatures ($\mathrm{TbNi}_{1-x}\mathrm{Sb}_2$, 5.6 K [10] or 12.0 K [7]; $\mathrm{TbCu}_{1-x}\mathrm{Sb}_2$, 9.0 K [7]). Inspection of the Weiss constants (Table 6) for different RE members shows a general trend that corresponds roughly to de Gennes scaling, indicating that RKKY interactions are the likely mechanism for magnetic coupling between the RE moments.

The magnetic data for $RE\mathrm{Zn}_{1-x}\mathrm{Sb}_2$ are similar to other $REM_{1-x}\mathrm{Sb}_2$ series (M = Ni, Pd, Cu, Ag, Au), which are also generally antiferromagnetic with low ordering temperatures ($T_N < 20$ K) that follow approximately de Gennes scaling [7–10]. In all these cases, the generally good agreement between the observed effective magnetic moments for $REM_{1-x}\mathrm{Sb}_2$ and the free-ion values for RE^{3+} implies that there is little or no contribution from the M atoms, consistent with the d^{10} configuration that is expected to be attained for M^{2+} (e.g., Zn^{2+}) or M^{+} (e.g., Cu^{+}) species.

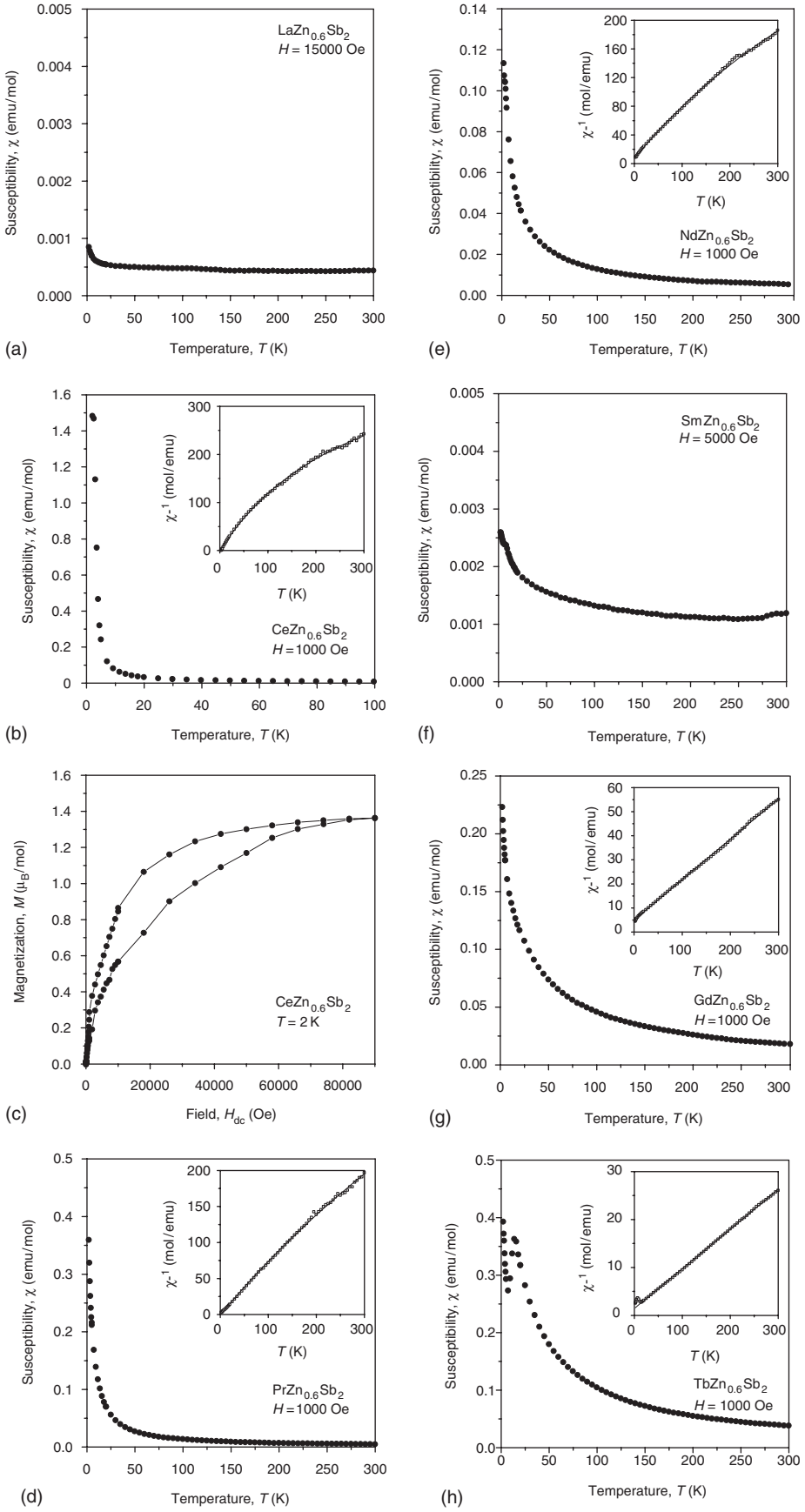

Fig. 4. Magnetic data for $RE\mathrm{Zn}_{0.6}\mathrm{Sb}_2$. The insets show the inverse susceptibility and fits to the modified (RE = Ce, Pr, Nd) or simple Curie–Weiss law (RE = Gd, Tb). The isothermal magnetization at 2 K for $\mathrm{CeZn}_{0.6}\mathrm{Sb}_2$ is shown in (c).

Acknowledgments

The Natural Sciences and Engineering Research Council of Canada and the University of Alberta supported this work. We thank Dr. Robert McDonald and Dr. Michael J. Ferguson (X-ray Crystallography Laboratory) for the X-ray data collection and Ms. Christina Barker (Department of Chemical and Materials Engineering) for assistance with the EDX analysis.

References

[1] G.S. Nolas, D.T. Morelli, T.M. Tritt, Annu. Rev. Mater. Sci. 29 (1999) 89–116.
[2] O.L. Sologub, P.S. Salamakha, in: K.A. Gschneidner Jr., J.-C.G. Bünzli, V.K. Pecharsky (Eds.), Handbook on the Physics and Chemistry of Rare Earths, vol. 33, Elsevier, Amsterdam, 2003, pp. 35–146.
[3] A.T. Nientiedt, W. Jeitschko, J. Solid State Chem. 142 (1999) 266–272.
[4] R. Demchyna, J.P.F. Jemetio, Yu. Prots, Th. Doert, L.G. Akselrud, W. Schnelle, Yu. Kuz'ma, Y. Grin, Z. Anorg. Allg. Chem. 630 (2004) 635–641.
[5] O. Sologub, K. Hiebl, P. Rogl, O. Bodak, J. Alloys Compd. 227 (1995) 40–43.
[6] S.K. Malik, Z. Chu, A.G. Joshi, J.B. Yang, W.B. Yelon, Q. Cai, W.J. James, K. Kamaraju, J. Appl. Phys. 91 (2002) 7842–7844.
[7] O. Sologub, K. Hiebl, P. Rogl, H. Noël, O. Bodak, J. Alloys Compd. 210 (1994) 153–157.
[8] O. Sologub, H. Noël, A. Leithe-Jasper, P. Rogl, O.I. Bodak, J. Solid State Chem. 115 (1995) 441–446.
[9] K.D. Myers, S.L. Bud'ko, I.R. Fisher, Z. Islam, H. Kleinke, A.H. Lacerda, P.C. Canfield, J. Magn. Magn. Mater. 205 (1999) 27–52.
[10] E.L. Thomas, M. Moldovan, D.P. Young, J.Y. Chan, Chem. Mater. 17 (2005) 5810–5816.
[11] A.V. Tkachuk, O.Ya. Zelinska, A. Mar, J. Solid State Chem. 179 (2006) 1506–1512.
[12] H. Flandorfer, O. Sologub, C. Godart, K. Hiebl, A. Leithe-Jasper, P. Rogl, H. Noël, Solid State Commun. 97 (1996) 561–565.
[13] G. Cordier, H. Schäfer, P. Woll, Z. Naturforsch. B: Anorg. Chem. Org. Chem. 40 (1985) 1097–1099.
[14] P. Wollesen, W. Jeitschko, M. Brylak, L. Dietrich, J. Alloys Compd. 245 (1996) L5–L8.
[15] L.P. Salamakha, S.I. Mudryi, J. Alloys Compd. 359 (2003) 139–142.
[16] T. Park, V.A. Sidorov, H. Lee, Z. Fisk, J.D. Thompson, Phys. Rev. B 72 (2005) 060410-1–060410-4.
[17] Y. Chen, J. Y. Lynn, H. Lee, P. Klavins, Z. Fisk, S. Nakatsuji, W. Bao, J. Thompson, T. Park, R. Macaluso, J. Chan, B. Carter, Bulletin of the American Physical Society, 2006 American Physical Society Meeting, March 13–17, 2006, Session W45.
[18] G.M. Sheldrick, SHELXTL, Version 6.12, Bruker AXS Inc., Madison, WI, 2001.
[19] L.M. Gelato, E. Parthé, J. Appl. Crystallogr. 20 (1987) 139–143.
[20] M. Brylak, M.H. Möller, W. Jeitschko, J. Solid State Chem. 115 (1995) 305–308.
[21] W. Tremel, R. Hoffmann, J. Am. Chem. Soc. 109 (1987) 124–140.
[22] G. Busch, O. Marinček, A. Menth, O. Vogt, Phys. Lett. 14 (1965) 262–264.